Raindrop size distribution and radar parameters at Cape Verde

A. Nzeukou, Henri Sauvageot, A.-D. Ochou, C.-M.-F. Kebe

Raindrop Size Distribution and Radar Parameters at Cape Verde

ARMAND NZEUKOU* AND HENRI SAUVAGEOT

Laboratoire d'Aérologie, Observatoire Midi-Pyrénées, Université Paul Sabatier, Toulouse, France

ABE DELFIN OCHOU

Université de Cocody, Abidjan, Ivory Coast

CHEIKH MOUHAMED FADEL KEBE

Université Cheikh Anta Diop, Dakar, Senegal

(Manuscript received 10 April 2002, in final form 28 July 2003)

ABSTRACT

Precipitation measurement using passive or active microwaves from space- or ground-based radar involves hypotheses about the raindrop size distribution (DSD). A universal knowledge of DSD characteristics is needed. A 4-yr dataset collected with a disdrometer at Dakar, Senegal, on the Atlantic coast of West Africa is used to analyze the DSD at the end of the continental trajectory of Sahelian squall lines. The DSDs are stratified in eight rain-rate classes and are fitted to analytical distributions. The shape of the averaged DSDs is found to be very similar from one year to the next. From rain rates R higher than about 20 mm h^{-1}, the slope of the DSDs tends toward a constant value. The coefficients of the Z–R relation, between the radar reflectivity factor Z and R, are different for convective and stratiform parts of the squall lines. However, because the Z–R relations for convective rain intersect the relation for stratiform rain for high rates, it is suggested that using a single Z–R relation enables correct representation of the whole Z and R range of variation in West Africa. The coefficients of this single Z–R are close to that of the stratiform relation and to that observed in other West African areas. The conditional probability density function of rain rate, $P(R)$, is of lognormal shape and also is very stable year after year. The coefficient of variation of R is found to be constant and close to 2.24, the value observed at many other sites. From $P(R)$, the linear coefficient $S(\tau)$ of the relation that links the area-averaged rain rate to the fractional area where the rain rate is higher than the threshold τ is computed and is found to be very stable for the values of τ close to m_R, the mean climatic value of R (around 5–6 mm h^{-1}). Because most of the sub-Saharan West African sites have a similar m_R, comparison shows that $S(\tau)$ is homogeneous over this area. This result suggests that $S(\tau)$ can be used with confidence for average rainfall estimation over a climatically homogeneous region.

1. Introduction

The raindrop size distribution (DSD) is pivotal in many areas related to precipitation remote sensing, as well as in several other environmental topics, such as telecommunications, precipitation scavenging, and soil erosion. Indeed most of the basic parameters used in these fields are deduced from the DSD and its moments. As an example, for the microwave remote sensing of precipitation, the coefficients of the relation Z–R between the radar reflectivity factor Z (mm^6 m^{-3}) and the rain rate R (mm h^{-1}), depend on the DSD (e.g., Ulbrich 1983; Feingold and Levin 1986; Sauvageot and Lacaux 1995; Atlas et al. 1999, 2000; Tokay et al. 1999, 2001). The DSD also determines the microwave radiometric brightness temperature T_B (K), the attenuation A (dB km^{-1}), and the optical extinction E (km^{-1}), as well as the liquid water content W (g m^{-3}). The rain-rate profile retrieval algorithms from space radar or from multichannel radiometric sensors, such as the Special Sensor Microwave Imager (SSM/I) on the Defense Meteorological Satellite Program (DMSP) and the Tropical Rainfall Measuring Mission (TRMM) Microwave Imager (TMI), are, thus, shown to be strongly affected by the DSD parameters (e.g., Coppens and Haddad 2000; Coppens et al. 2000; Viltard et al. 2000; Iguchi et al. 2000).

In fact, to respond in a satisfactory way to the needs recalled above, notably for precipitation remote sensing,

* Current affiliation: IUT Fotso Victor, Université de Dschang, Bandjoun, Cameroon.

Corresponding author address: Dr. Henri Sauvageot, Université Paul Sabatier, Laboratoire d'Aérologie, Observatoire Midi-Pyrénées, 65300 Lannemezan, France.
E-mail: sauh@aero.obs-mip.fr

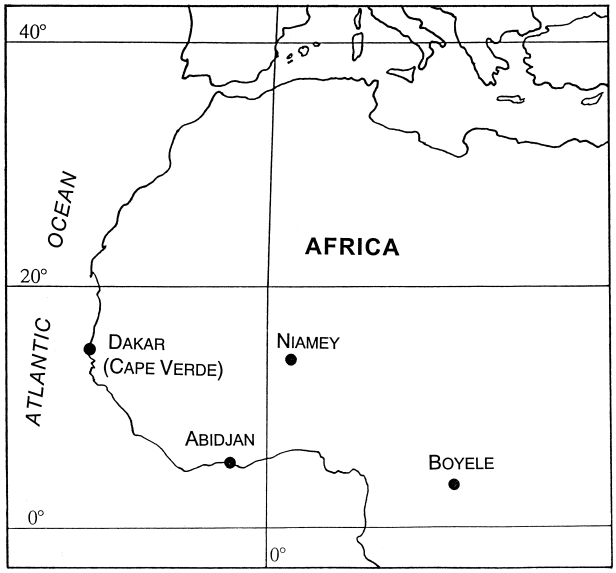

FIG. 1. Location of the data collection sites.

a functional description of DSD, usable in all points of the earth's atmosphere, should be known. Such a DSD parameterization is not available on a global basis and this lack jeopardizes rain field retrieval accuracy from space.

The cause of this lack of global knowledge of DSD is clearly that the conditions influencing the DSD are not completely analyzed and that their contribution is not correctly quantified and parameterized, for lack of the requisite observational field data. The main conditions that are known (or can be suspected) to have a significant influence on the shape, and then on the parameters deduced from the DSD, are, among others, the ones that influence the convection and the precipitation growth, namely the latitude, orographic effects, humidity flux, and maybe maritime or continental character, because atmospheric stability and, thus, convection are different over sea than over land, as suggested by the land–sea difference in the lightning activity (Zipser 1994; Christian et al. 1999; Boccippio et al. 2000; Seity et al. 2001). Moreover Iguchi et al. (2000) suggest, from the TRMM observations, that there could be some changes in the DSD associated with the convective rain over sea with that over land. The tropical latitudes are particularly interesting to document, because of the quantitative importance of precipitation and energetic transfer that takes place there. Now, despite that, tropical latitude DSDs are poorly documented, notably in Africa, because of the scarcity of observational sites.

The goal of the present paper is to analyze 4 yr of data on the DSDs collected with a disdrometer at Dakar (Cape Verde), Senegal (Fig. 1), on the Atlantic coast of West Africa. The only published DSDs for central and West Africa are (Fig. 1) from Niamey (Niger), Boyélé (Congo), and Abidjan (Ivory Coast) (Sauvageot and Lacaux 1995). The originality of Dakar, with respect to the other observed areas, is that it is the most western land site of Africa on the westward trajectory of the Soudano-Sahelian squall lines (Desbois et al. 1988; Nzeukou and Sauvageot 2002). After the description of the dataset, the main results about the shape of the DSDs stratified by rain-rate classes, the coefficients of the Z–R relation, and the probability distribution function of the rain rate are presented and compared with those of the other sites.

2. Data

The data were collected at Dakar (14°34′N, 17°29′W), Senegal. Dakar is located at the headland of Cape Verde (Fig. 1). The climate of this area is Sahelian with a rainy season reduced to about 3 months, from early July to late September, when the intertropical convergence zone (ITCZ) is higher than 13°N. Radar and satellite observations show that most of the rain-bearing systems crossing this area are organized as squall lines that become weaker and then disappear as they migrate from land to sea and move over the nearby ocean. However, inversely, a few systems grow stronger, advance over the sea and could be involved in the genesis of the hurricanes of the west tropical Atlantic (e.g., Gray and Landsea 1992). The Dakar area is flat over several hundred kilometers, with an altitude lower than 200 m. The mean annual cumulative rainfall at Dakar is about 500–600 mm, with a strong meridional gradient. Nzeukou and Sauvageot (2002) found, from an analysis of radar data, that the rain field around Dakar is approximately ergodic.

DSDs were observed with a Joss and Waldvogel (1967) disdrometer (JWD hereinafter). The JWD enables measurements of the size distribution of raindrops by converting the mechanical moment of falling drops into electric pulses. The performances and limitations of this widely used sensor are well known and have been discussed in many papers (e.g., Joss and Waldvogel 1969; McFarquhar and List 1993; Sheppard 1990; Sheppard and Joe 1994; Sauvageot and Lacaux 1995; Tokay et al. 2001; see, also, online at http://www.distromet.com). Only drops with an equivalent spherical diameter D larger than 0.3 mm are detected. In the JWD used, the pulses are converted to eight-bit numbers and sorted according to 25 size classes, all with the same width ($\Delta D = 0.2$ mm), covering diameters ranging from 0.3 to 5.3 mm. It is acknowledged that, in heavy rainfall, small drops ($D < 1$ mm) are not accurately counted with JWD because of instrumental shortcomings. However, Sauvageot and Lacaux (1995) present arguments showing that the relatively low number of small drops usually observed in tropical rain is partly real when the JWD is carefully used from a site from which the sources of microphonic noise are removed. The data were processed for a (partial) correction of the error due to the dead time of the instrument after the sampling area is hit by a drop, using the method proposed by the

manufacturer. Details on the JWD measurement limits are out of the scope of the present paper and can be found in the above-quoted references. The measurement time span of a DSD is 1 min. Disdrometers are very efficient for the measurement of low rain rates, which is important for an accurate estimation of the mean rain rate.

The JWD was set on the flat roof of the building housing the Laboratory for Atmospheric Physics Simeon Fongang (LPASF) at the Ecole Supérieure Polytechnique of the University Cheikh Anta Diop of Dakar. This roof is about 10 m above the ground and is covered with a nonnoisy asphalted material and a piece (2 m × 2 m) of moquette. No microphonic noise sources were present close to the JWD. The disdrometer was regularly calibrated using man-made drops of a known size (created with vibrating hypodermic syringes). The calibrations do not show any drift of the JWD characteristics during the period of the observations.

The observations were activated only during the rainy season, which is between early June and late October. The data sample used is made up of 4 yr of observations, from 1997 to 2000, as described in Table 1. Because of human-caused problems, the convective parts of some squall lines (about 30%) were not correctly observed in 1999 (the device protecting the sensor was belatedly removed after the beginning of the rain), so that the sample for this particular year gives an erroneous apportionment between convective and stratiform rain, as well as an insufficient cumulative rainfall and mean convective rain rate. The total sample consists of 10 359 DSDs of 1 min, that is 172.6 h of rain observation, with a cumulative rainfall of 976 mm.

3. Convective and stratiform areas

The conditional (i.e., when raining) average rain rate measured at Dakar with the JWD is 5.68 mm h^{-1} (without 1999), compatible with the average rain rate obtained for the Dakar region from 7 yr of Dakar–Yoff (Senegal) radar data, which is 5.08 and 5.11 mm h^{-1}, for the sea and land areas, respectively (Nzeukou and Sauvageot 2002). These values are also very close to those observed at Niamey (5.14 mm h^{-1}), Boyélé (5.51 mm h^{-1}), and Abidjan (4.52 mm h^{-1}; Sauvageot 1994), showing that the average rain rate is homogeneous through West Africa.

In Table 1, and hereinafter, a distinction is made between the convective and stratiform areas of the squall lines, as is frequently done in the literature on tropical rain. Such a distinction is justified by the fact that, in the tropical squall lines, and notably in Sahelian squall lines (e.g., Gamache and Houze 1982; Tokay and Short 1996; Ramos-Buarque and Sauvageot 1997; Sauvageot and Koffi 2000; Atlas et al. 2000), convective and stratiform areas appear clearly separated, the first with a high and strongly varying rain rate, and the second with a low and more uniform rain rate.

TABLE 1. The dataset. Convective area and stratiform area correspond to DSDs with rain-rate R higher and lower than 10 mm h^{-1}, respectively; H is the cumulative rainfall height of the rain season; C/all is the ratio of convective to convective + stratiform; and Σ is the summation of the 4 yr 1997–2000. The year 1999 is not complete.

Year	No. of rain events	No. of 1-min DSD in the sample				H (mm)				R_{mean} (mm h^{-1})			R_{max} (mm h^{-1})
		All	Convective area	Stratiform area	C/all (%)	All	Convective area	Stratiform area	C/all (%)	All	Convective area	Stratiform area	
1997	32	2546	362	2184	14	239	177	62	74	5.63	29.38	1.69	100
1998	38	3560	485	3075	14	362	249	113	69	6.11	30.85	2.20	127
1999	31	4052	289	3763	7	246	130	116	53	3.64	26.98	1.85	129
2000	47	4253	529	3724	12	375	274	101	73	5.30	31.11	1.64	124
Σ	148	10 359*	1376*	8983*	13	976*	700*	276*	72	5.68*	29.58	1.85	129

* Without 1999.

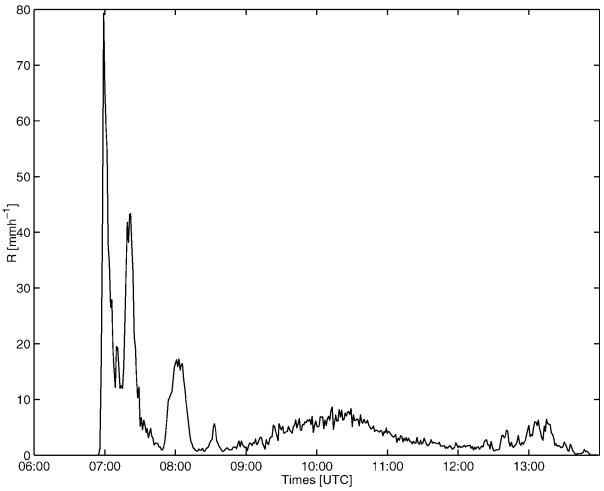

FIG. 2. Hyetograph of the squall line of 16 Sep 1998 observed at Dakar with a JWD. Time: h and min.

Figure 2 shows the example of a Sahelian squall line hyetograph observed at Dakar with the JWD. Three convective rain cells crossed over the JWD between 0657 and 0815 UTC. The convective line is observed between 0657 and 0730 UTC, that is, about 0.5 h. A third rain cell, around 0800 UTC, seems located within the transition region, which is rather unusual. After 0815 UTC, a stratiform region lasting for 5 h, with a rain rate less than 10 mm h^{-1}, is observed. Figure 3 presents the DSDs associated with the first rain cell, between 0657 and 0708 UTC. It displays the typical evolution through a convective line (Sauvageot and Koffi 2000; Atlas and Ulbrich 2000), notably for the shapes and slopes of the successive DSDs; at the beginning, in the part where R is increasing, the DSDs are multimodal, with gentle slope, a low drop number, and a high reflectivity factor due to the presence of large drops. Then, in the part where R is decreasing, the DSDs display steep slopes, with a high drop number and a low reflectivity factor because drops are smaller than about 3 mm. If, for example, the DSD is compared at 0657 and 0708 UTC,

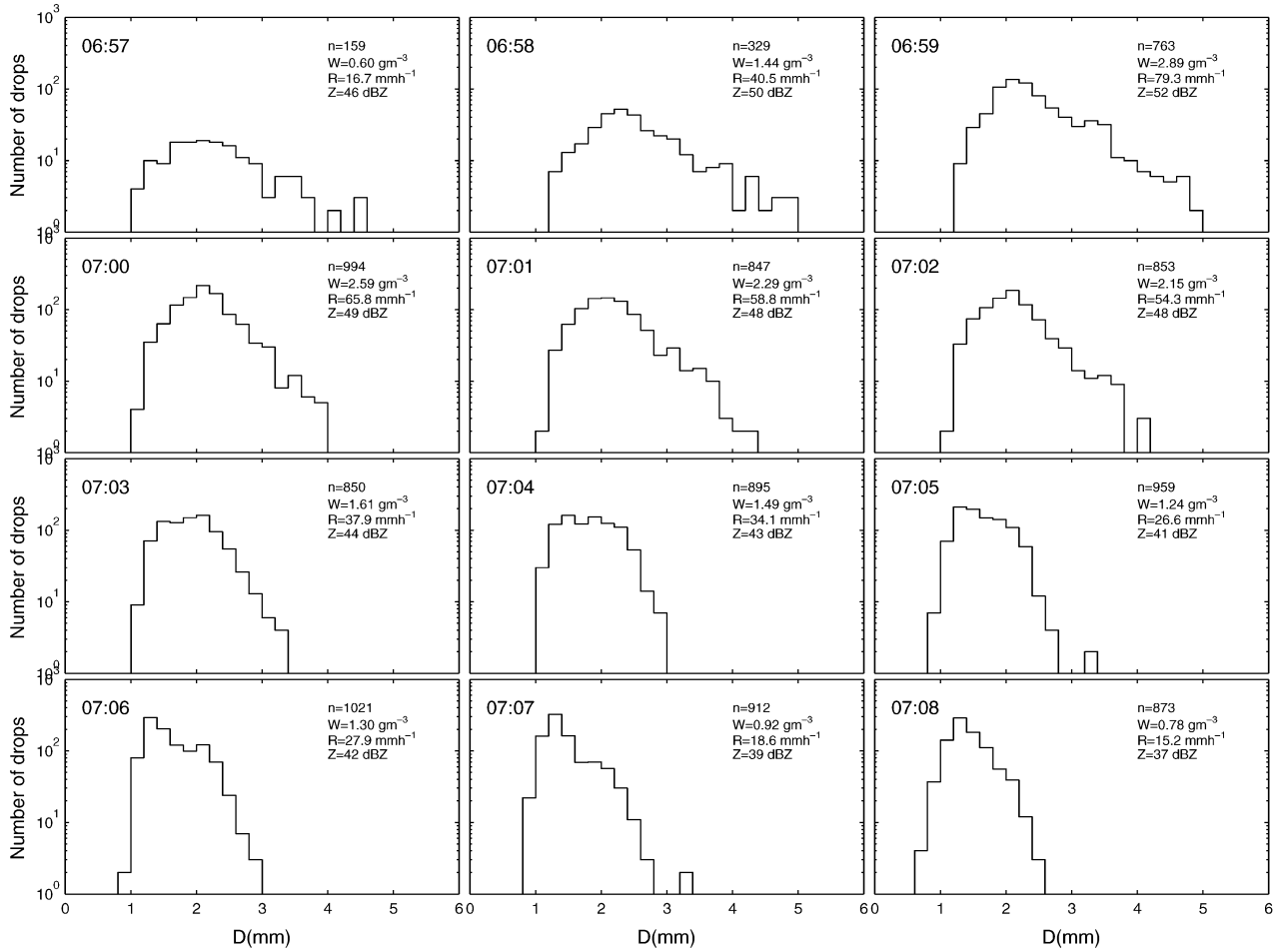

FIG. 3. Drop size distribution observed at the beginning of the squall line of Fig. 2, corresponding to the first peak of the hyetogram. Respectively, n, W, R, and Z are the observed drop number, liquid water content, rain rate, and radar reflectivity factor.

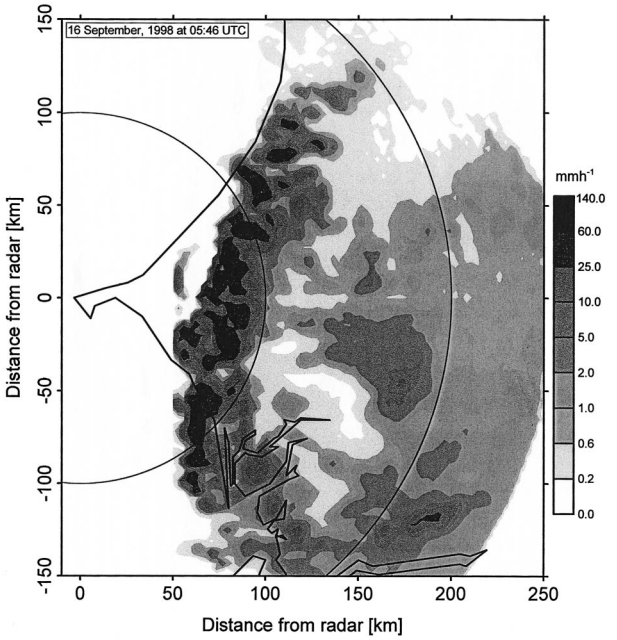

FIG. 4. Distribution of the rain rate deduced from the radar data collected with radar of Dakar–Yoff at 0546 UTC 16 Sep 1998.

for almost the same rain rate, the drop number increases by a factor of 5.5 and Z decreases by 9 dB.

Figure 4 is the corresponding plan position indicator (PPI) of the rain rate computed from the radar reflectivity factor observed at 0546 UTC, when the leading edge of the squall line was about 50 km east of Dakar. For the computation we have used the general Z–R relation given in section 5. The average velocity of the squall line, between 0546 UTC and its arrival over the JWD, is about 43 km h^{-1}, which is slower than the usual value of the Sahelian squall line velocity (about 60 km h^{-1}; Desbois et al. 1988). Usually the Sahelian squall line velocity decreases when moving from land to sea. The organization displayed on Fig. 4 is very typical of a Sahelian squall line, with, from west to east, a convective line of intense rain cells, a minimum (or transition) reflectivity zone, and a wide stratiform area, which also appears on the hyetograph.

Most authors have found that DSDs of convective and stratiform areas display some differences, namely, that the slope is steeper for convective than for stratiform DSDs and, consequently, that the drop number concentration is higher and the median volume diameter (D_0) is smaller for convective than for stratiform DSDs, respectively. They also observed that, in the stratiform area, a fraction of the DSDs display shape characteristics similar to that of the convective area (Tokay and Short 1996; Yuter and Houze 1997; Tokay et al. 1999; Atlas et al. 1999, 2000). The convectivelike character of these stratiform area DSDs seems to be associated with the presence of updrafts embedded in the stratiform cloud deck (as observed by aircraft or wind profiler; Tokay et al. 1999; Atlas et al. 1999, 2000), or to decreasing rain-rate sequences (Sauvageot and Koffi 2000), as illustrated in Fig. 3.

In the present paper, we do not discuss the partition of stratiform DSDs in DSDs having a stratiform- or a convectivelike character (this topic will be tackled in a companion paper). We consider here only the distinction between convective and stratiform areas, which is the only distinction that can be done from the usual panoramic (i.e., PPI) radar data.

To delimit the convective and stratiform areas, the division can logically be taken at the minimum of reflectivity of the transition zone. However, the transition zone is not always as easily located as in Figs. 2 and 4. That is why the criterion of the minimum of reflectivity cannot be applied in an automatic way. To define an automatic criterion, it can be observed, in Fig. 2 and most of the tropical squall line hyetograms (e.g., Gamache and Houze 1982; Tokay and Short 1996; Tokay et al. 1999; Sauvageot and Koffi 2000; Atlas et al. 2000), that the rain rate in the stratiform area is usually lower than 10 mm h^{-1} (or about 38 dBZ), while it is always higher than that in the convective line. Using $R = 10$ mm h^{-1} as a criterion to delimit convective and stratiform rain leads also to undue integration of the DSDs of the convective line, which are <10 mm h^{-1}, into the stratiform sample. It can be observed, however, that the number of DSDs affected by this miscount is very small and is associated with a very small rainfall amount. Moreover, this criterion puts the transition zone into the stratiform sample when the transition zone seems, at least for the DSD characteristics, to be different for the convective and stratiform parts (Atlas et al. 1990). In the present work, the criterion $R = 10$ mm h^{-1} has been used to delimit convective and stratiform rain.

Table 1 shows that the cumulative rainfall is 72% and 28% for the convective and stratiform parts, respectively, though distributed over a DSD number of 13% and 87%, respectively. These proportions are comparable with those found, using the same criterion, by Tokay and Short (1996) on an atoll of the equatorial West Pacific (namely, 68% for convective and 32% for stratiform).

The rainy events numbered in Table 1 are defined as a period over which the rain is observed at the ground by the JWD with no interruption longer than 1 h. In fact, at Cape Verde, in most cases, a rainy event is associated with a squall line.

4. DSD stratified by rain-rate classes

The concept of averaged DSD is legitimate only inside rain-rate classes because most DSD parameters depend not only on rain rates, such as, for example, the slope in the exponential or gamma distributions (e.g., Ulbrich 1983), but also on the drop number or the shape parameter. That is why the data of each of the 4 yr of observation and the whole dataset (Σ) were stratified

TABLE 2. Coefficients of the moments of $N(D)$ such as defined by relation (1).

Parameter	Symbol P	p	Unit	a_P
Rain rate	R	3.67	mm h^{-1}	7.1×10^{-3}
Liquid water content	W	3	g m^{-3}	$(\pi/6) \times 10^{-3}$
Radar reflectivity factor	Z	6	mm^6 m^{-3}	1

into eight classes of rain rate in order to compute some integral parameters. The integral parameters P are the rain rate R and the radar reflectivity factor Z, with the definition

$$P = a_P \int_0^\infty D^p N(D)\, dD, \tag{1}$$

where $N(D)$ is the number of raindrops per unit volume, per unit size interval (mm^{-1} m^{-3}), D is the equivalent spherical diameter (mm), and a_P is a coefficient depending on the parameter definition and on the units, such as those given in Table 2. Coefficient p in (1) results from the definition of the parameters; Z and R are the 6- and 3.67-order moments of D, respectively, where 3.67 comes from the product of D^3 and $D^{0.67}$, corresponding to the drop volume and drop terminal velocity (Atlas and Ulbrich 1977), respectively.

In Table 3, the limits of the classes and the numerical values of the integral parameters are given with, in addition, the median volume diameter D_0 and the modal diameter D_m.

The observed distributions were fitted to the three most often used analytical forms. The fitted parameters are given in Table 3. These forms are

1) exponential (Marshall and Palmer 1948):

$$N(D) = N_0 \exp(-\lambda D), \tag{2}$$

where N_0 (mm^{-1} m^{-3}) is the intercept and λ is the slope of the distribution;

2) gamma modified (Ulbrich 1983):

$$N(D) = N_0 D^\mu \exp(-\Lambda D), \tag{3}$$

where N_0 ($mm^{-1-\mu}$ m^{-3}) is related to the drop number, μ is a shape parameter, and Λ (mm^{-1}) is the slope; and

3) lognormal (e.g., Feingold and Levin 1986; Sauvageot and Lacaux 1995):

$$N(D) = \frac{N_T}{(2\pi)^{0.5}(\ln\sigma)D} \exp\left[-\frac{\ln^2(D/D_g)}{2\ln^2\sigma}\right], \tag{4}$$

where N_T (m^{-3}) is the total number of drops, D_g (mm) is the mean geometrical diameter, and σ is the standard geometrical deviation of D.

In order to emphasize the dependency of the slope parameter on rain rate, only the drops with a diameter larger than D_m were considered in the fitting to the exponential distribution. The gamma-modified parameters were computed using the method of moments (e.g., Kozu and Nakamura 1991; or Tokay and Short 1996). The lognormal parameters are obtained simply using the definition formulas.

Table 3 is organized analogously with that presented by Sauvageot and Lacaux (1995) for other African sites, in order to make comparison easy.

Figure 5 presents the observed drop size distributions for the eight rain-rate classes. The usual small misrepresentations associated with the defects of the transfer function of the JWD are observed. Notably the classes with central values of 1.0 and 2.0 mm display some bumps (Sheppard 1990), and the drop number increases in the last class (5.1–5.3 mm), from the counting in that class of all the drops having $D > 5.1$ mm (including the drops larger than 5.3 mm). Figure 5 also displays the deficit in small drops, with respect to the exponential, sometimes observed in the DSDs of the tropical latitudes (Ulbrich 1983; Feingold and Levin 1986; Sauvageot and Lacaux 1995; Tokay and Short 1996; Atlas et al. 1999; Atlas and Ulbrich 2000; and others).

The shape of the DSDs is remarkably alike for the 4 yr of the dataset and for the merged sample. To emphasize this similarity, the different distributions for three rain-rate classes were superimposed on the same graph (Fig. 6). The agreement is very good. On Fig. 5, for 1999, the slope of the class $R \geq 60$ mm h^{-1} is less steep than for the other years. The explanation is probably in the low number of DSDs available in the corresponding class (only 15, due to the human-caused problem pointed out in section 2), leading to a high variance. The similarity of the DSD shapes for the 4 yr shows that the precipitation growth conditions remain also very similar from one year to the next. Such a conclusion is compatible with the ergodicity of the rain field as emphasized by Nzeukou and Sauvageot (2002).

Several authors have discussed the relation between R and the parameters of the analytic distributions used to fit the observed DSDs (e.g., Ulbrich 1983; Feingold and Levin 1986; Sauvageot and Lacaux 1995, among others) without leading to universal conclusions, either on the best shape or on the influence of R on the parameters. It was also suggested that, with the increase of R, and then with the increase of the number of drop interactions within the falling rain, the DSDs could evolve toward an unvarying shape, thus, independent from R. In such conditions, $N(D)$ would be a linear function of R, that is, $N(D) = R\,\psi(D)$, where $\psi(D)$ is a shape function of universal character. This relation implies that, for heavy rain (i.e., $R > 20$ mm h^{-1}), the moments of $N(D)$ are linear functions of R, and that the relation between the moments is also linear. Notably, the Z–R relation has the form $Z = aR$, where a is a coefficient (List 1988; see also Atlas and Ulbrich 2000). To document these various points, the parameters of distributions in (2), (3), and (4), fitted to the stratified DSDs of Fig. 5 and Table 3, are plotted in Fig. 7. The curves fitted to the data are drawn in Fig. 7, and the

TABLE 3. Parameters of the averaged DSDs for 4 yr of Table 1 and for the whole dataset Σ; R, W, Z, D_0, and D_m are the rain rate, liquid water content, radar reflectivity factor, median volume diameter, and modal diameter, respectively; N_0 and λ are the parameters of the exponential distribution (2) obtained by regression on the classes whose size is larger than the mode of the distribution; ρ is the correlation coefficient; N_0, Λ, and μ are the parameters of the gamma distribution (3); N_T, D_g, and σ are the parameters of the lognormal distribution (4).

									Exponential			Gamma			Lognormal		
Year	Sample name	Class of rain rate (mm h^{-1})	No. of DSD of 1 min	R (mm h^{-1})	W (g m^{-3})	Z (dbZ)	D_0 (mm)	D_m (mm)	N_0 (mm^{-1} m^{-})	λ (mm^{-1})	ρ	N_0 (mm$^{-1-\mu}$ m^{-3})	Λ (mm^{-1})	μ	N_T (m^{-3})	D_g (mm)	σ
1997	R_1	$R < 2$	1579	0.6	0.034	24.7	1.19	0.80	438	2.68	0.97	2883	4.2	1.9	51	0.99	1.42
	R_2	$2 \le R < 4$	323	2.9	0.14	33.3	1.56	1.00	1820	2.50	0.99	4639	3.7	2.4	123	1.17	1.45
	R_3	$4 \le R < 6$	143	4.8	0.23	36.0	1.59	1.00	2697	2.44	0.98	4941	3.3	1.9	181	1.21	1.44
	R_4	$6 \le R < 10$	139	7.8	0.37	38.3	1.51	1.20	2329	2.21	0.96	4480	2.6	0.6	291	1.23	1.39
	R_5	$10 \le R < 20$	162	13.8	0.65	40.4	1.64	1.20	6546	2.39	0.97	17 579	3.6	2.5	410	1.33	1.38
	R_6	$20 \le R < 40$	124	29.4	1.27	45.0	1.89	1.20	9450	2.19	0.97	17 596	3.4	3.1	526	1.53	1.38
	R_7	$40 \le R < 60$	36	47.5	1.91	48.3	2.13	1.20	8822	1.93	0.97	13 489	3.6	4.5	520	1.74	1.38
	R_8	$60 \le R$	40	76.4	3.05	50.0	2.15	2.00	163 358	2.66	0.99	38 145	4.9	7.7	726	1.85	1.34
1998	R_1	$R < 2$	1853	0.7	0.042	25.0	1.17	0.80	2297	3.44	0.99	9337	5.1	3.1	63	1.00	1.40
	R_2	$2 \le R < 4$	634	2.9	0.15	31.7	1.32	1.00	6269	3.20	0.99	28 750	5.2	4.0	150	1.14	1.37
	R_3	$4 \le R < 6$	327	5.0	0.24	34.6	1.48	1.20	24 022	3.46	0.99	46 198	5.4	5.0	191	1.24	1.37
	R_4	$6 \le R < 10$	261	7.5	0.37	36.2	1.47	1.20	35 147	3.47	0.99	121 261	6.0	5.9	271	1.28	1.34
	R_5	$10 \le R < 20$	229	14.2	0.68	39.7	1.59	1.20	18 433	2.87	0.98	79 658	5.1	4.9	413	1.37	1.32
	R_6	$20 \le R < 40$	137	27.5	1.20	43.9	1.86	1.20	18 224	2.48	0.99	62 394	5.0	6.1	474	1.58	1.32
	R_7	$40 \le R < 60$	53	48.1	1.98	47.1	2.03	2.00	144 083	2.85	0.99	80 192	6.0	9.3	522	1.82	1.30
	R_8	$60 \le R$	66	81.7	3.16	50.9	2.26	2.00	66 091	2.29	0.99	20 874	4.9	8.3	577	2.05	1.29
1999	R_1	$R < 2$	2452	0.8	0.043	25.6	1.19	0.80	1317	3.13	0.99	5408	4.5	2.5	67	0.98	1.43
	R_2	$2 \le R < 4$	878	2.8	0.14	32.4	1.41	1.00	4235	2.96	0.99	10 131	4.3	3.0	141	1.13	1.42
	R_3	$4 \le R < 6$	275	4.8	0.23	35.3	1.59	1.00	8613	2.98	0.99	15 101	4.5	3.9	172	1.25	1.41
	R_4	$6 \le R < 10$	159	7.7	0.38	36.6	1.48	1.20	14 714	3.03	0.99	61 684	5.3	4.8	285	1.27	1.35
	R_5	$10 \le R < 20$	134	14.2	0.66	39.8	1.66	1.20	17 332	2.82	0.99	107 319	5.7	6.2	370	1.40	1.34
	R_6	$20 \le R < 40$	100	28.0	1.19	44.3	1.93	1.20	16 177	2.42	0.99	48 986	5.1	6.7	408	1.65	1.33
	R_7	$40 \le R < 60$	40	49.0	2.01	47.2	2.04	2.00	128 971	2.81	0.99	74 142	5.9	9.1	528	1.82	1.30
	R_8	$60 \le R$	15	75.6	2.85	52.1	2.36	2.00	7323	1.59	0.95	5244	2.7	3.5	482	2.05	1.32
2000	R_1	$R < 2$	2814	0.6	0.034	23.9	1.17	0.80	2036	3.52	0.99	9419	5.3	3.3	53	0.98	1.42
	R_2	$2 \le R < 4$	401	2.9	0.16	31.3	1.22	1.00	8605	3.33	0.99	27 156	4.9	3.2	186	1.09	1.37
	R_3	$4 \le R < 6$	240	4.9	0.25	34.6	1.40	1.20	5840	2.85	0.98	26 591	4.7	3.7	217	1.20	1.38
	R_4	$6 \le R < 10$	269	7.7	0.38	36.7	1.46	1.20	15 276	3.03	0.99	38 699	4.8	3.9	304	1.23	1.37
	R_5	$10 \le R < 20$	209	14.1	0.68	39.3	1.55	1.20	23 106	2.98	0.99	162 098	5.8	5.9	450	1.33	1.34
	R_6	$20 \le R < 40$	194	28.6	1.28	43.5	1.79	1.20	34 752	2.77	0.99	141 325	5.7	6.8	576	1.51	1.33
	R_7	$40 \le R < 60$	72	48.8	2.03	47.1	1.97	1.40	39 063	2.49	0.99	69 545	5.3	7.6	579	1.77	1.29
	R_8	$60 \le R$	54	82.1	3.23	50.1	2.17	2.00	293 126	2.84	0.99	65 264	6.4	11.4	630	2.03	1.26
Σ	R_1	$R < 2$	8698	0.7	0.038	24.8	1.18	0.80	1072	3.12	0.99	6084	4.8	2.7	59	0.99	1.42
	R_2	$2 \le R < 4$	2236	2.9	0.15	32.2	1.36	1.00	4173	2.96	0.99	12 166	4.4	3.0	149	1.13	1.40
	R_3	$4 \le R < 6$	985	4.9	0.24	35.0	1.50	1.00	6925	2.91	0.99	17 860	4.5	3.6	191	1.23	1.39
	R_4	$6 \le R < 10$	828	7.6	0.37	36.9	1.48	1.20	6686	2.70	0.98	26 875	4.4	3.4	288	1.25	1.36
	R_5	$10 \le R < 20$	734	14.1	0.67	39.8	1.61	1.20	12 560	2.69	0.98	61 372	4.9	4.5	415	1.35	1.34
	R_6	$20 \le R < 40$	555	28.4	1.24	44.1	1.86	1.20	15 661	2.41	0.98	48 245	4.6	5.2	509	1.55	1.34
	R_7	$40 \le R < 60$	201	48.4	1.99	47.3	2.02	2.00	56 085	2.52	0.99	46 318	5.0	7.2	543	1.79	1.31
	R_8	$60 \le R$	175	80.1	3.13	50.6	2.21	2.00	58 072	2.28	0.99	24 941	4.7	7.7	619	1.99	1.30

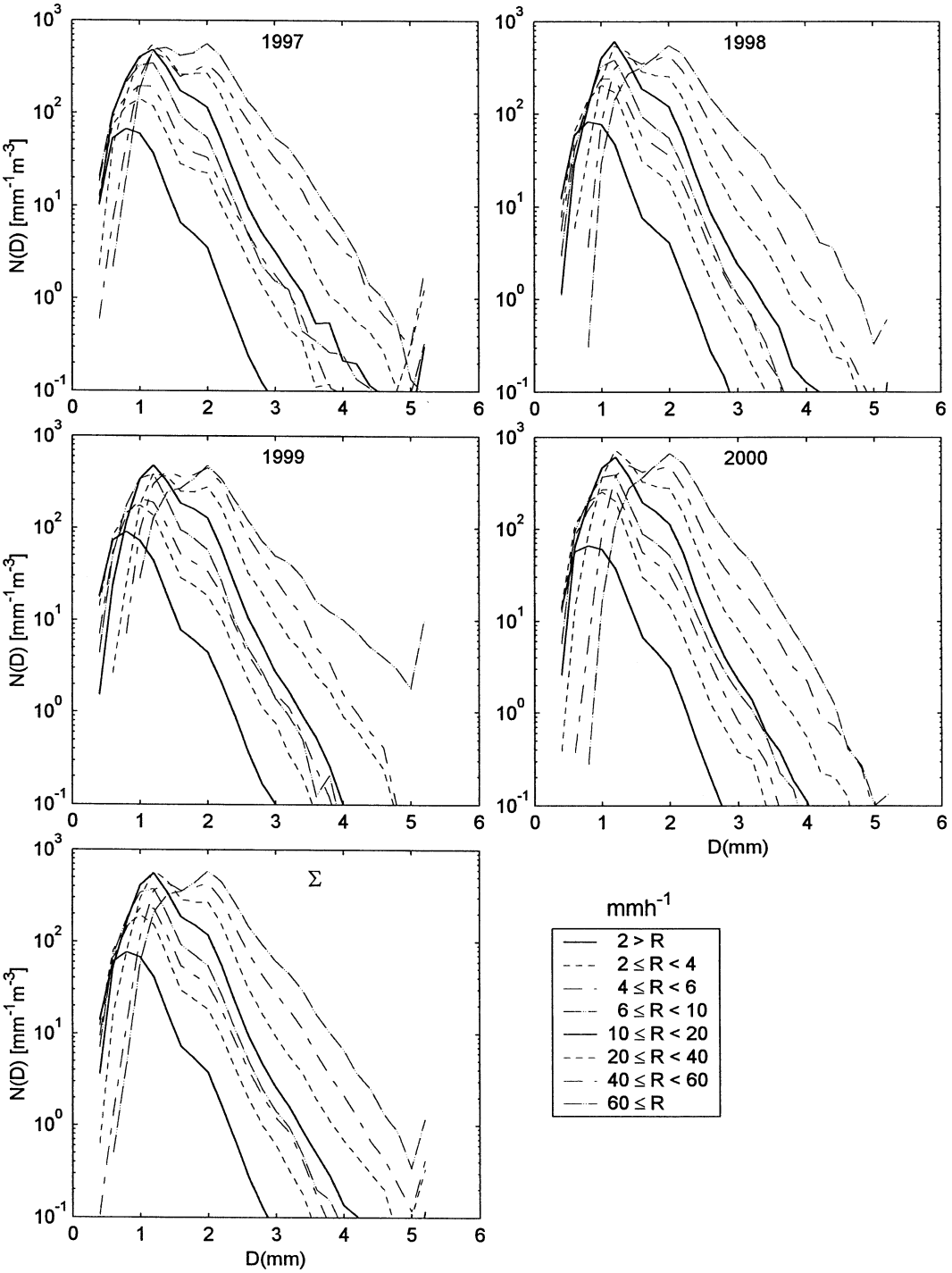

FIG. 5. Averaged DSDs for the 4 yr of Table 1 and for the whole dataset Σ.

corresponding equations are given in Table 4. The relations are not very tight, except for lognormal distributions because of the logarithmic compression of the variation. The coefficients are close to those obtained for other West African areas (Sauvageot and Lacaux 1995; Table 3).

The intercept and drop number parameters, N_0 and N_T, and the shape parameters, μ and D_g, increase with R. However, the rate of variation is much lower for R larger than 10 mm h^{-1}, that is, for convective rain. This kind of evolution with R is particularly clear with the slope λ but with a decrease with R. For R higher than 20 mm h^{-1}, λ tends toward a constant value around 2.5 mm^{-1}. Similar observations were related by Mueller and

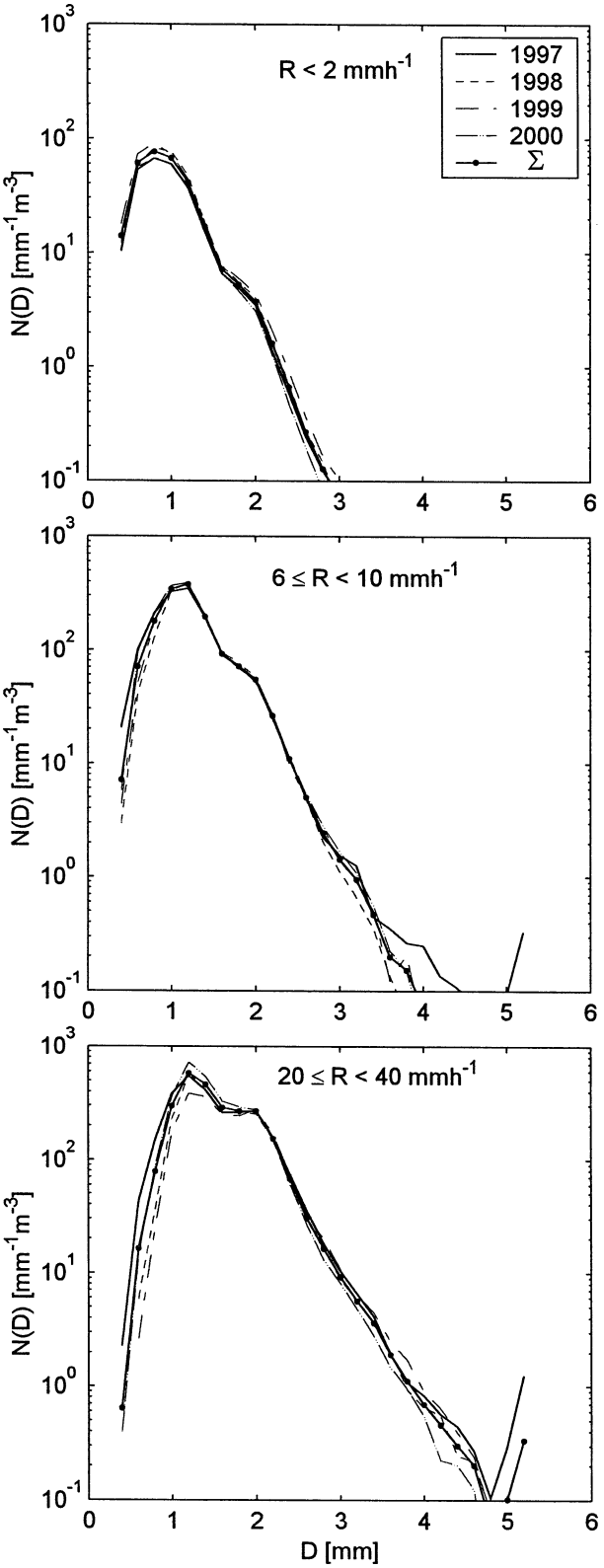

FIG. 6. Superimposition of the averaged DSDs for the three classes.

Sims (1966), Sekhon and Srivastava (1971), Pasqualucci (1982), and Sauvageot and Lacaux (1995) we find that Λ and σ are almost independent from R. The above results are not sufficient to reach a conclusion about the validity of the universal $\psi(D)$ concept. They show, however, that, with increasing R, the parameters of tropical DSDs tend toward weakly varying values.

Comparing the values of the fitted parameters (Table 3) with those obtained at other sites in West Africa by Sauvageot and Lacaux (1995), shows that the DSDs from Dakar are closer to those of Abidjan on the Gulf of Guinea coast near the equator, than to those of Niamey, located at the same latitude but in the continental area. This comparison is illustrated in Table 5 where D_0 and the parameters of the lognormal distribution for the various sites are given for $R > 20$ mm h^{-1}.

5. *Z–R* relations

As is well known, the radar reflectivity factor of rain and rain rate are linked by a relation of the form

$$Z = aR^b, \tag{5}$$

where a and b are coefficients depending on the DSD (cf. section 1), that is, on the condition of precipitation growth, mainly the depth and intensity of the convection (e.g., Dotzek and Beheng 2001). In tropical precipitation, and notably in tropical squall lines, a distinction is often made between convective and stratiform *Z–R* relations owing to the differences between the rain rate observed in the corresponding areas, as discussed in section 3.

Table 6 gives the values of coefficients a and b of (5) computed by least squares fitting. Figure 8 shows, as an example, the data point and the fitted line for 2000. It can be seen that the number of data points for $R <$ 1 mm h^{-1} is higher than that for $R > 1$ mm h^{-1}. However, because their number and their spreading over more than two size orders in dBR [R (mm h^{-1}) in dBR $= 10 \log_{10}$] and three in dBZ, the points for $R < 1$ mm h^{-1} can be suspected to strongly influence the *Z–R* relation for higher rain rate. That is why a class $R > 1$ mm h^{-1} is considered in Table 6, in addition to the convective and stratiform area classes, corresponding to $R \geq 10$ mm h^{-1} and $R < 10$ mm h^{-1}, respectively. The corresponding size of the data samples and cumulative rain are given in Table 1. Figure 9 shows the data points and fitted curves for the 4 yr and for the merged sample. For the sake of clarity, only 1 point for 10 and 1 point for 20 are plotted for the convective and stratiform rain rate, respectively.

The scatter of the annual values of b in Table 6 appears to be very small within a same category (less than 7% and 5% for convective and stratiform, respectively). The scatter of the annual values of a is larger (up to 42% and 27% for convective and stratiform, respectively).

As observed for other areas on tropical rain systems,

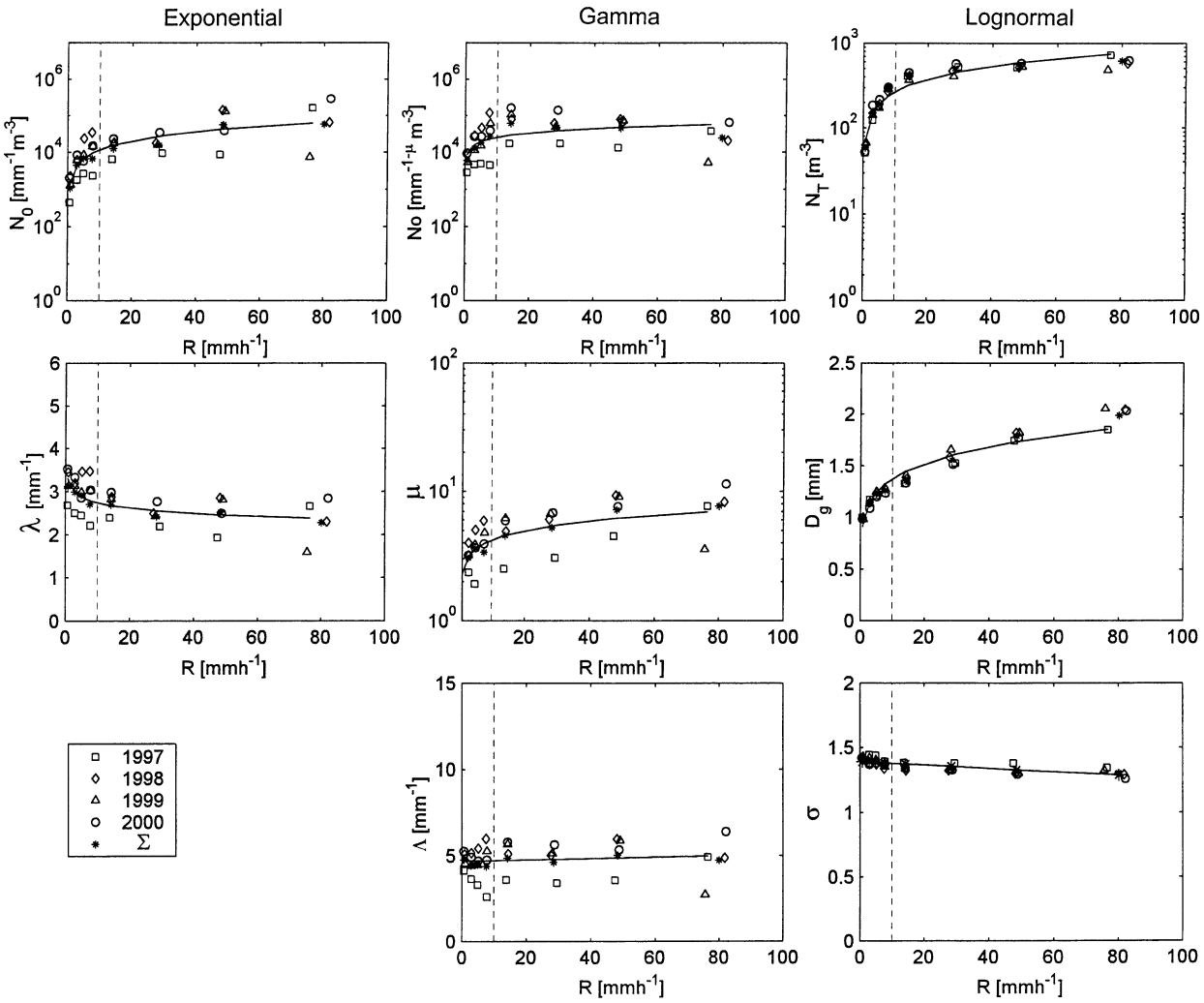

FIG. 7. Variation of the exponential, gamma, and lognormal parameters as a function of the rain rate R. The parameters are defined in (2), (3), and (4) respectively. The dashed vertical line shows the 10 mm h^{-1} rain-rate threshold.

notably on squall lines (e.g., Tokay and Short 1996; Tokay et al. 1999; Atlas and Ulbrich 2000; Atlas et al. 1999, 2000), the intercept a and the power coefficient b are smaller and higher, respectively, for convective than stratiform rain. The intercept for stratiform rain is twice as large as the convective value. Similar coefficients were obtained by Tokay and Short (1996) in the tropical Pacific, namely, $Z = 367\ R^{1.30}$ for stratiform and $Z = 139\ R^{1.43}$ for convective. In Table 6 the b coefficient for stratiform rain is observed to be smaller than that for convective rain by about 16% in such a way that the Z–R curves intersect around 30 mm h^{-1}, or 44 dBZ. Atlas and Ulbrich (2000) found the con-

TABLE 4. Analytical function fitted between the parameters of the three distributions of Table 3 and the rain rate R. The data points used for the fitting and the fitted curves are shown in Fig. 7. Units are as in Table 3.

Exponential	Gamma	Lognormal
	$N_0 = 10\ 528R^{0.39}$	$N_T = 86R^{0.50}$
$N_0 = 1865R^{0.81}$	$\rho = 0.50$	$\rho = 0.97$
$\rho = 0.80$		
	$\mu = 2.43R^{-0.24}$	$D_g = 0.98R^{0.15}$
$\lambda = 3.2R^{-0.07}$	$\rho = 0.61$	$\rho = 0.97$
$\rho = 0.50$		
	$\Lambda = 4.68 + 0.004R$	$\sigma = 1.39 - 0.0013R$
	$\rho = 0.11$	$\rho = 0.73$

TABLE 5. Comparison of the average of the drop mean volume diameter D_0 and lognormal distribution parameters N_T, D_g, and σ, for the various sites and for $R > 20$ mm h^{-1}. The data from Abidjan and continental Africa (i.e., Niamey + Boyélé) are taken from Sauvageot and Lacaux (1995; Table 2).

	D_0	N_T	D_g	σ
Dakar	2.03	557	1.78	1.32
Abidjan	2.16	515	1.67	1.34
Niamey + Boyélé	2.36	326	2.03	1.27

TABLE 6. Parameters of relation $Z = aR^b$ between the radar reflectivity factor Z and the rain rate R for the 4 yr of Table 1 and for the whole dataset Σ; ρ is the correlation coefficient.

	Convective area ($R > 10$ mm h^{-1})			Stratiform area ($R > 0$ mm h^{-1}			Stratiform area ($R > 1$ mm h^{-1})			All ($R > 0$ mm h^{-1})			All ($R > 1$ mm h^{-1})		
Year	a	b	ρ	a	b	ρ	a	b	ρ	a	b	ρ	a	b	ρ
1997	205	1.43	0.88	405	1.28	0.95	420	1.26	0.80	397	1.25	0.97	428	1.22	0.93
1998	144	1.51	0.93	351	1.24	0.95	361	1.21	0.83	350	1.24	0.97	345	1.25	0.94
1999	146	1.53	0.90	387	1.25	0.94	404	1.22	0.77	385	1.24	0.95	401	1.22	0.90
2000	153	1.46	0.91	352	1.22	0.95	351	1.20	0.82	351	1.22	0.97	337	1.23	0.94
Σ	162	1.48	0.91	371	1.24	0.95	385	1.21	0.80	368	1.24	0.97	375	1.22	0.93

vergence of the Z–R relations at $R \approx 50$ mm h^{-1}. The determination of the convergence point is not very accurate.

The a and b coefficients for the total sample (i.e., without distinction between convective and stratiform areas), as well as the sample for $R > 1$ mm h^{-1}, are almost the same as for the coefficient for the stratiform area (difference of less than 5% and 2% for a and b, respectively). Although corresponding to a small cumulative rain, the stratiform sample is associated with a large number of data points.

Figure 10 shows the Z–R relations for the 4 yr and for the merged sample Σ. The Z–R curves for stratiform and for both (stratiform and convective) areas are superimposed and independent from the year. Because of the small differences in b coefficients and the intersection of the curves around 30–50 mm h^{-1}, the spacing between the convective curves and the others is significant only for the small values of R, a region where the convective data points are rare and associated with very small rain amounts. That is why in West Africa using a single Z–R relation (i.e. without making a distinction between convective and stratiform areas) is acceptable

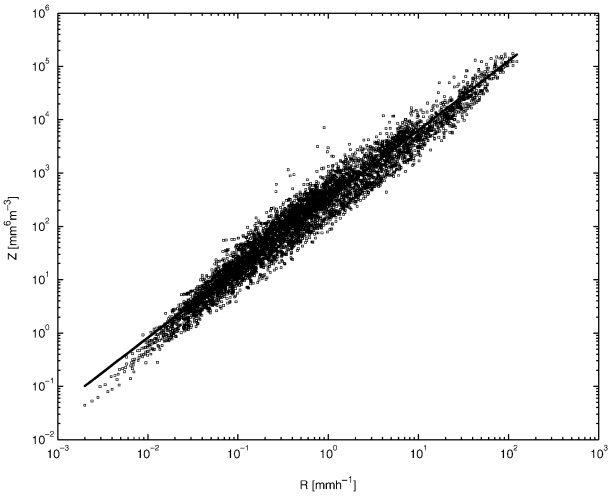

FIG. 8. Radar reflectivity factor Z vs rain rate R as deduced from the 1-min DSDs observed with the JWD at Dakar, during 2000, and fitted curve. The equation of the fitted curve is $Z = 351R^{1.22}$ (see Table 6).

to process all the data points, including the convective component.

The more general relation for the Dakar area is

$$Z = 368R^{1.24} \tag{6}$$

(Z: mm^6 m^{-3}, and R: mm h^{-1}).

Relations between integral parameters can also be obtained from (1) (e.g., Ulbrich 1983; Feingold and Levin 1986; Sauvageot and Lacaux 1995). Using (4) in (1), assuming that the DSDs are lognormal, and integrating for Z and R, gives, with the coefficients of Table 2,

$$Z = N_T D_g^6 \exp(18 \ln^2 \sigma), \tag{7}$$

$$R = 7.1 \times 10^{-3} N_T D_g^{3.67} \exp(6.73 \ln^2 \sigma). \tag{8}$$

Eliminating σ between (7) and (8), we have

$$Z = 5.6 \times 10^5 N_T^{-1.675} D_g^{-3.82} R^{2.67}. \tag{9}$$

Replacing N_T and D_g in (9) by their expression in function of R given in Table 4 leads to

$$Z = 355R^{1.26}, \tag{10}$$

which is very close to (6).

Sauvageot and Lacaux (1995; Table 3) obtained Z–R relations very similar to that at Dakar from the regression of JWD data for equatorial West Africa ($Z = 369R^{1.28}$) and continental West Africa ($Z = 364R^{1.36}$). All of this suggests that a relation with a mean coefficient, such as

$$Z = 368R^{1.30}, \tag{11}$$

is reasonable to represent the rain, without the convective–stratiform distinction in tropical West Africa, but with, however, some reservation concerning the areas strongly affected by orographic effect. In this case are the two places where the maxima of cumulative rainfall for West Africa—almost 10 m yr^{-1}—are observed, namely, in Conakry, Guinea, which is southwest of Fouta Djalon (11°20′N, 12°10′W), and southwest Cameroon, southwest of Mont Cameroon, for which no DSD observations are available.

6. Probability density function of rain rate

An important characteristic of a rain field is the conditional probability distribution function (pdf) of the

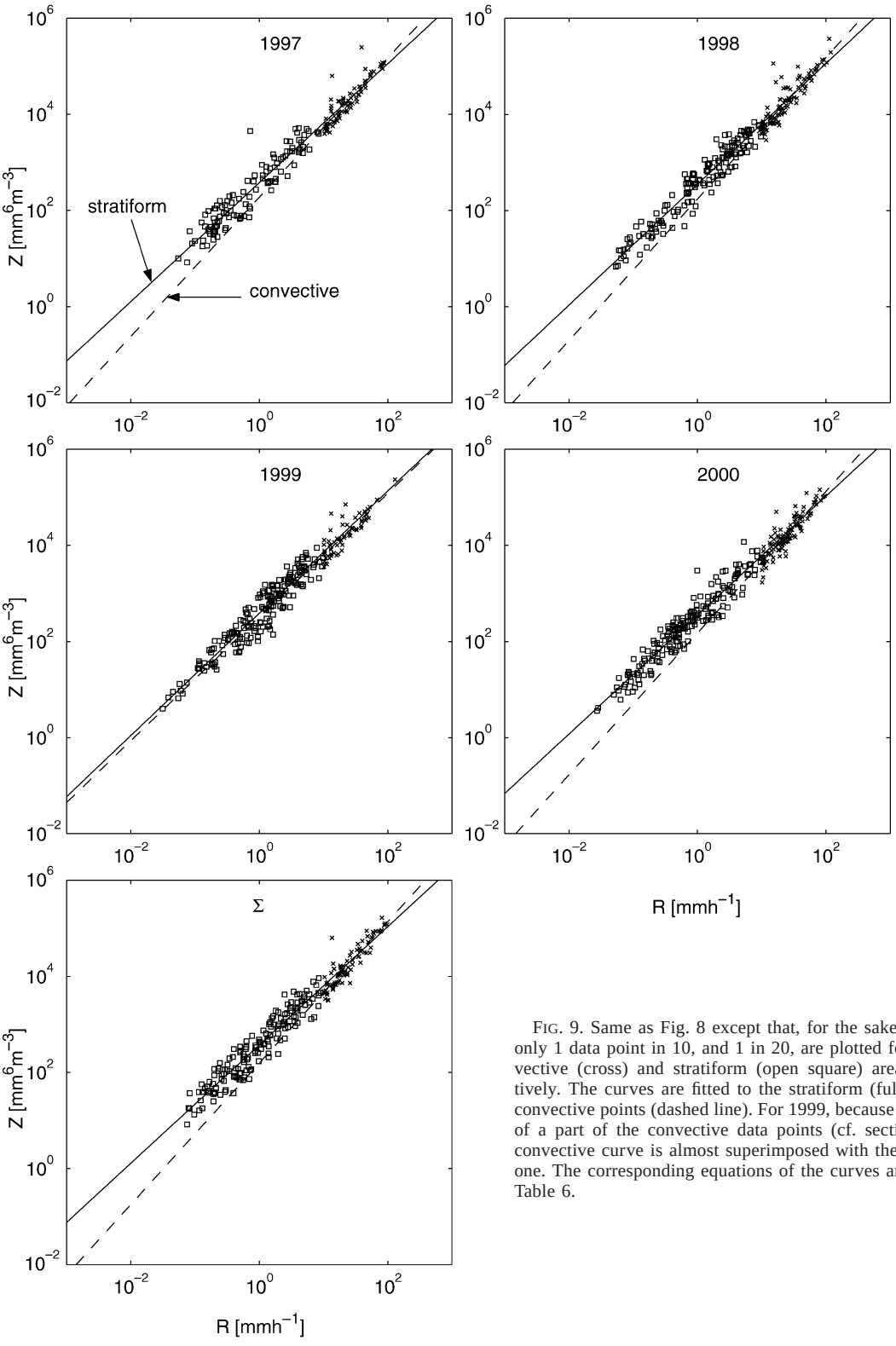

FIG. 9. Same as Fig. 8 except that, for the sake of clarity, only 1 data point in 10, and 1 in 20, are plotted for the convective (cross) and stratiform (open square) areas, respectively. The curves are fitted to the stratiform (full line) and convective points (dashed line). For 1999, because of the lack of a part of the convective data points (cf. section 2), the convective curve is almost superimposed with the stratiform one. The corresponding equations of the curves are given in Table 6.

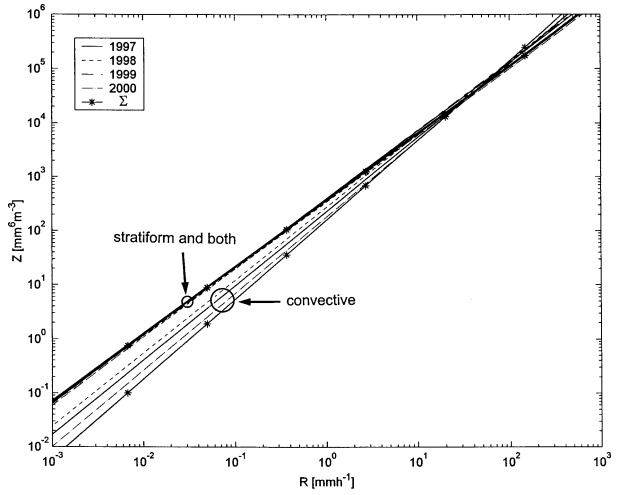

FIG. 10. Comparison between the Z–R curves of Fig. 9 and Table 6.

rain rate, $P(R)$, for $R > 0$, notably because $P(R)$ plays a part in the estimation of the area average rain rate from the threshold methods (e.g., Atlas et al 1990; Atlas and Bell 1992; Sauvageot et al. 1999).

Figure 11 shows the pdf of R computed from the JWD data of Dakar for the 4 yr of Table 1 and for the merged sample. With a lognormal distribution $P(R)$ can be represented (Atlas et al. 1990; Kedem et al. 1990; Sauvageot 1994). A lognormal probability distribution is determined by two parameters, the mean m and the variance σ^2. Table 7 gives the value of the mean and variance of R, that is, m_R and σ_R^2 and that of the transformed variable $Y = \ln R$, that is, m_Y and σ_Y^2. Table 7 also gives the coefficient of skewness γ_1 and of kurtosis (or flatness) γ_2 of the pdf, which expresses the deviation of the computed curves with respect to a perfect Gaussian curve.

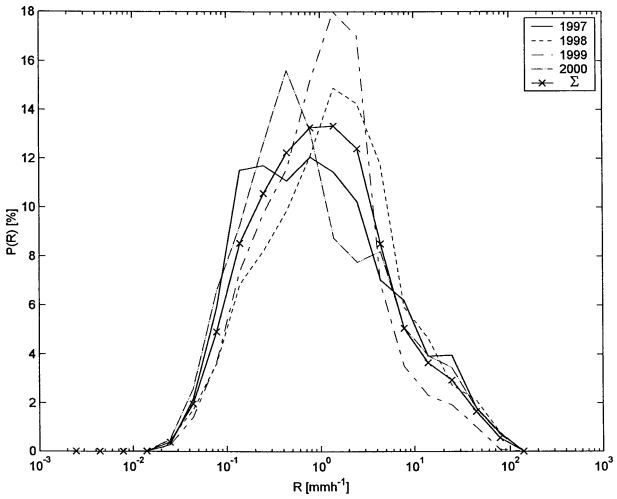

FIG. 11. Probability density function of the rain rate for the 4 yr of Table 1 and for the whole dataset.

TABLE 7. The lognormal distribution parameters fitted to the curves of Fig. 11 and the $S(\tau)$ values for the 4 yr of Table 1 and for the whole dataset Σ; γ_1 and γ_2 are the skewness and kurtosis, respectively; m_R, σ_R^2, M_Y, and σ_Y^2 are the mean and the variance of R and of $Y = \ln R$, respectively; CV is the coefficient of variation m_R/σ_R; τ is the rain threshold.

Year	γ_1	γ_2	m_r (mm h^{-1})	σ_r^2 (mm h^{-1})^2	CV	m_Y	σ_Y^2	$S(\tau)$ for τ = 0.5	1	2	4	6	8	10	20
1997	0.36	−0.6	5.63	156	2.22	0.84	1.78	8.53	10.81	14.90	22.37	28.76	34.31	39.80	72.05
1998	0.07	−0.3	6.11	181	2.20	0.93	1.76	7.84	9.49	12.81	20.38	29.31	38.50	45.09	85.42
1999	0.12	−0.03	3.64	66	2.23	0.40	1.79	4.83	6.12	9.28	20.55	33.16	42.09	51.41	95.85
2000	0.45	−0.43	5.30	157	2.36	0.73	1.88	8.13	11.32	15.77	21.86	28.43	36.01	42.89	70.90
Σ	0.26	−0.35	5.09	138	2.31	0.71	1.84	7.14	9.15	12.92	21.23	29.61	37.46	44.34	79.30

The annual curves, in Fig. 11, show some variability of the modal size—on the right for 1998, and on the left for 1997 and 2000. The curve for 1999 also displays an undercounting of the high rain rate, as pointed out in section 2. The curve for the merged sample is Gaussian-shaped. In Table 7, the skewness is almost zero, showing that the curves are symmetrical, and the kurtosis is slightly negative, that is, the curves are slightly platykurtic, as observed in other African areas (Sauvageot 1994). The pdfs of Fig. 11 are, thus, reasonably well represented by lognormal distributions. The values of m_R, m_Y, σ_R^2, and σ_Y^2 are very close to those observed in two other African areas, that is, Abidjan and Niamey (Fig. 1), showing a high degree of rain field homogeneity for sub-Saharan West Africa.

The coefficient of variation CV $= m_R/\sigma_R$ (cf. Table 7) is found to be almost constant from year to year and is very close to 2.24. This value was previously observed at several sites (Sauvageot 1994), and computed from radar data in the area of Dakar (Nzeukou and Sauvageot 2002).

Knowledge of $P(R)$ enables us to compute $S(\tau)$, the coefficient of proportionality between the area-averaged rain rate $\langle R \rangle$ and the fractional area $F(\tau)$ occupied by the rain with a rate higher than a threshold τ. It is found (Doneaud et al. 1984; Atlas et al. 1990) that one can write

$$\langle R \rangle = S(\tau)F(\tau), \tag{12}$$

with $\langle R \rangle = \int_0^\infty RP(R)\, dR$ and $F(\tau) = \int_\tau^\infty P(R)\, dR$, in such a way that

$$S(\tau) = \int_0^\infty RP(R)\, dR \Big/ \int_\tau^\infty P(R)\, dR. \tag{13}$$

Using (13), the coefficient $S(\tau)$ was computed for various values of the threshold τ, between 0.5 and 20 mm h^{-1}. The results are given in Table 7. Comparison of the values for Dakar with those of the other African sites of Fig. 1 (cf. Sauvageot 1994; Table 2) shows that the annual values of $S(\tau)$, for τ around the mean climatic value m_R (cf. Table 7 or Table 1), that is, 5–6 mm h^{-1}, are stable and very close for the various sites of observation, around 26, as illustrated by Fig. 12 where the curves of $S(\tau)$ for these various places are drawn. This shows that the relation (12) is very homogeneous for West Africa, owing to the ergodicity of the rain fields, and that the method of rain-rate estimation from fractional area $F(\tau)$ is very sound.

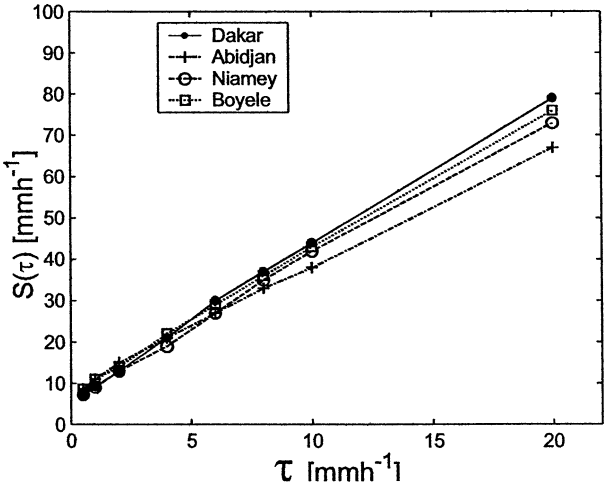

FIG. 12. Comparison of the curves $S(\tau)$ for the Dakar area and for three other sites of West Africa.

7. Summary and conclusions

A dataset of 148 rain events, collected with a disdrometer at Dakar on the Atlantic coast of West Africa between 1997 and 2000, was used to study the characteristics of the raindrop size distribution at the transition between land and sea. Most of these rain systems are Sahelian squall lines moving westward, made up of an intense convective line followed by a wide stratiform area. The convective rain area is found to represent about 13% of rain duration, but 72% of the cumulative rainfall (about 325 mm). The average rain rate is 5.7 mm h^{-1}, very close to the values observed in other West African areas.

The DSDs were stratified into eight rain-rate classes and were fitted to exponential, gamma, and lognormal distributions. The shape of the annually averaged DSDs is very alike from one year to the next. Comparison with the shapes observed in two other places of West Africa, namely, Niamey, located at the same latitude as Dakar in the continental Sahel, and Abidjan, on the coast of the Gulf of Guinea, shows that although the DSDs are very close for the three sites, those of Dakar are more similar to those of Abidjan than those of Niamey, suggesting that the coastal influence could be stronger than that of latitude.

The variation of the parameters of the fitted distributions, as a function of R, shows that for R larger than about 20 mm h^{-1}, the shape of the DSD changes much more slowly than for smaller R values, as observed in other places. Notably, the slope tends toward a constant value.

The radar reflectivity factor–rain-rate (Z–R) relation is found to be different for convective and stratiform areas, with linear and power coefficients smaller and higher, respectively. Now, because of the high number of data points associated with stratiform area, the Z–R relation obtained without making any convective–stratiform area distinction is very similar to the stratiform-only one. The result is that Z–R curves for convective and stratiform areas are found to intersect at a rain rate around 30–50 mm h^{-1}, in such a way that the Z–R relation, without a convective–stratiform area distinction, closely represents not only the low but also the high rain rate. Then it is concluded that, in West Africa,

distinguishing between convective and stratiform area Z–R relations does not seem to be very useful.

Comparison with results from other places suggests that a relation of the form $Z = 368R^{1.30}$ (Z: mm^6 m^{-3}, R: mm h^{-1}) stands for all the sub-Saharan West Africa.

The conditional probability density function of rain rate $P(R)$ (for $R > 0$) at Dakar is also very similar from one year to the next and is lognormally shaped. The coefficient of variation is found to be almost constant around 2.31, that is, very close to the value of 2.24 (or $\sqrt{5}$) observed in several sites.

The linear coefficient $S(\tau)$ of the relation that links the area-averaged rain rate and the fractional area where the rain rate is higher than the threshold τ, was computed from $P(R)$. Like $P(R)$, $S(\tau)$ for the Dakar area is very stable, notably near $\tau = \mu_R$, the mean value of R. In West Africa, μ_R is about 5–6 mm h^{-1}. Around this value of μ_R, the coefficient $S(\tau)$ is also very homogeneous for the various sites of West Africa. This result suggests that a unique $S(\tau)$ coefficient can be used for the estimation of $\langle R \rangle$ from $F(\tau)$ in most places of tropical West Africa.

Acknowledgments. The authors are grateful to all of those who contributed to the collecting of the dataset used in this study, that is, the team of the Laboratoire de Physique de l'Atmosphère Simeon Fongang (LPASF) of the Ecole Supérieure Polytechnique, University Cheikh Anta Diop at Dakar, under the leadership of Professor Simeon Fongang (now deceased).

REFERENCES

Atlas, D., and C. W. Ulbrich, 1977: Path- and area-integrated rainfall measurement by microwave attenuation in the 1–3 cm band. *J. Appl. Meteor.,* **16,** 1322–1331.

——, and T. L. Bell, 1992: The relation of radar to cloud area–time integrals and implications for rain measurements from space. *Mon. Wea. Rev.,* **120,** 1997–2008.

——, and C. W. Ulbrich, 2000: An observationally based conceptual model of warm oceanic convective rain in the Tropics. *J. Appl. Meteor.,* **39,** 2165–2181.

——, D. Rosenfeld, and D. A. Short, 1990: The estimation of convective rainfall by area integrals, 1, The theoretical and empirical basis. *J. Geophys. Res.,* **95** (D3), 2153–2160.

——, C. W. Ulbrich, F. D. Marks, E. Amitai, and C. R. Williams, 1999: Systematic variation of drop size and radar-rainfall relations. *J. Geophys. Res.,* **104** (D6), 6155–6169.

——, ——, ——, R. A. Black, E. Amitai, P. T. Willis, and C. E. Samsury, 2000: Partitioning tropical oceanic convective and stratiform rains by draft strength. *J. Geophys. Res.,* **105** (D2), 2259–2267.

Boccippio, D. J., S. J. Goodman, and S. Heckman, 2000: Regional differences in tropical lightning distributions. *J. Appl. Meteor.,* **39,** 2231–2248.

Christian, H., and Coauthors, 1999: Global frequency and distribution of lightning as observed by the Optical Transcient Detector (OTD). *Preprints, 11th Conf. on Atmospheric Electricity,* Guntersville, AL, NASA, 734–737.

Coppens, D., and Z. S. Haddad, 2000: Effects of raindrop size distribution variations on microwave brightness temperature calculation. *J. Geophys. Res.,* **105** (D19), 24 483–24 489.

——, ——, and E. Im, 2000: Estimating the uncertainty in passive-microwave rain retrievals. *J. Atmos. Oceanic Technol.,* **17,** 1618–1629.

Desbois, M., T. Kayiranga, B. Gnamien, S. Guessous, and L. Picon, 1988: Characterization of some elements of the Sahelian climate and their interannual variations. *J. Climate,* **1,** 868–904.

Doneaud, A. A., S. I. Niscov, D. L. Priegnitz, and P. L. Smith, 1984: The area–time integral as an indicator for convective rain volume *J. Climate Appl. Meteor.,* **23,** 555–561.

Dotzek, N., and K. D. Beheng, 2001: The influence of deep convective motions on the variability of Z–R relations. *Atmos. Res.,* **59,** 15–39.

Feingold, G., and Z. Levin, 1986: The lognormal fit to raindrop spectra from frontal convective clouds in Israel. *J. Climate Appl. Meteor.,* **25,** 1346–1363.

Gamache, J. F., and R. A. Houze, 1982: Mesoscale air motions associated with a tropical squall line. *Mon. Wea. Rev.,* **110,** 118–135.

Gray, W. M., and C. W. Landsea, 1992: African rainfall as a precursor of hurricane-related destruction on the U.S. East Coast. *Bull. Amer. Meteor. Soc.,* **73,** 1352–1364.

Iguchi, T., T. Kozu, R. Meneghini, J. Awaka, and K. Okamoto, 2000: Rain-profiling algorithm for the TRMM precipitation radar. *J. Appl. Meteor.,* **39,** 2038–2052.

Joss, J., and A. Waldvogel, 1967: Ein Spectrograph für Niederschlagstropfen mit automatisher Auswertung. *Pure Appl. Geophys.,* **68,** 240–246.

——, and ——, 1969: Raindrop size distribution and sampling size errors. *J. Atmos. Sci.,* **26,** 566–569.

Kedem, B., L. S. Chiu, and Z. Karni, 1990: An analysis of the threshold method for measuring area-average rainfall. *J. Appl. Meteor.,* **29,** 3–20.

Kozu, T., and K. Nakamura, 1991: Rainfall parameter estimation from dual-radar measurements combining reflectivity profile and path-integrated attenuation. *J. Atmos. Oceanic Technol.,* **8,** 259–271.

List, R., 1988: A linear radar reflectivity–rainrate relationship for steady tropical rain. *J. Atmos. Sci.,* **45,** 3564–3572.

Marshall, J. S., and W. M. K. Palmer, 1948: The distribution of raindrops with size. *J. Meteor.,* **5,** 165–166.

McFarquhar, G. M., and R. List, 1993: The effect of curve fits for the disdrometer calibration on raindrop spectra, rainfall rate, and radar reflectivity. *J. Appl. Meteor.,* **32,** 774–782.

Mueller, E. A., and A. L. Sims, 1966: Radar cross sections from drop size spectra. Illinois State Water Survey Tech. Rep. ECOM-00032F, 110 pp.

Nzeukou, A., and H. Sauvageot, 2002: Distribution of rainfall parameters near the coasts of France and Senegal. *J. Appl. Meteor.,* **41,** 69–82.

Pasqualucci, F., 1982: The variation of drop size distribution in convective storms: A comparison between theory and measurement. *Geophys. Res. Lett.,* **9,** 839–841.

Ramos-Buarque, S., and H. Sauvageot, 1997: The estimation of rainfall in the Sahelian squall-line by the area-threshold method. *Atmos. Res.,* **43,** 207–216.

Sauvageot, H., 1994: The probability density function of rain rate and the estimation of rainfall by area integrals. *J. Appl. Meteor.,* **33,** 1255–1262.

——, and J. P. Lacaux, 1995: The shape of averaged drop size distributions. *J. Atmos. Sci.,* **52,** 1070–1083.

——, and M. Koffi, 2000: Multimodal raindrop size distributions. *J. Atmos. Sci.,* **57,** 2480–2492.

——, F. Mesnard, and R. S. Tenorio, 1999: The relation between the area-average rain rate and the rain cell size distribution parameters. *J. Atmos. Sci.,* **56,** 57–70.

Seity, Y., S. Soula, and H. Sauvageot, 2001: Lightning and precipitation relationship in coastal thunderstorms. *J. Geophys. Res.,* **106** (D19), 22 801–22 816.

Sekhon, R. S., and R. C. Srivastava, 1971: Doppler observations of drop size distributions in a thunderstorm. *J. Atmos. Sci.,* **28,** 983–994.

Sheppard, B. E., 1990: Effect of irregularities in the diameter clas-

sification of raindrops by the Joss–Waldvogel disdrometer. *J. Atmos. Oceanic Technol.,* **7,** 180–183.
——, and P. I. Joe, 1994: Comparison of raindrop size distribution measurements by a Joss–Waldvogel disdrometer, a PMS 2DG spectrometer, and a POSS Doppler radar. *J. Atmos. Oceanic Technol.,* **11,** 874–887.
Tokay, A., and D. A. Short, 1996: Evidence from tropical raindrop spectra of the origin of rain from stratiform and convective clouds. *J. Appl. Meteor.,* **35,** 355–371.
——, ——, C. R. Williams, W. L. Eckland, and K. S. Gage, 1999: Tropical rainfall associated with convective and stratiform clouds: Intercomparison of disdrometer and profiler measurements. *J. Appl. Meteor.,* **38,** 302–320.
——, A. Kruger, and W. E. Krajewski, 2001: Comparison of drop size distribution measurements by impact and optical disdrometers. *J. Appl. Meteor.,* **40,** 2083–2097.
Ulbrich, C. W., 1983: Natural variations in the analytical form of the raindrop size distribution. *J. Climate Appl. Meteor.,* **22,** 1764–1775.
Viltard, N., C. Kummerov, W. S. Olson, and Y. Hong, 2000: Combined use of the radar and radiometer of TRMM to estimate the influence of drop size distribution on rain retrievals. *J. Appl. Meteor.,* **39,** 2103–2114.
Yuter, S. E., and R. A. Houze, 1997: Measurements of raindrop size distributions over the Pacific warm pool and implications for *Z–R* relations. *J. Appl. Meteor.,* **36,** 847–867.
Zipser, E. J., 1994: Deep cumulonimbus cloud systems in the Tropics with and without lightning. *Mon. Wea. Rev.,* **122,** 1837–1851.